Cirrus Cloud Properties Derived from POLDER-1/ADEOS Polarized Radiances: First Validation Using a Ground-Based Lidar Network

HÉLÈNE CHEPFER,* PHILIPPE GOLOUB,+ JAMES SPINHIRNE,# PIERRE H. FLAMANT,* MARIO LAVORATO,@ LAURENT SAUVAGE,* GÉRARD BROGNIEZ,+ AND JACQUES PELON&

* *Laboratoire de Météorologie Dynamique, École Polytechnique, Palaiseau, France*
+ *Laboratoire d'Optique Atmosphérique, Université Lille 1, Villeneuve d'Ascq, France*
# *NASA Goddard Space Flight Center, Greenbelt, Maryland*
@ *CEILAP, Villa Martelli, Argentina*
& *Service d'Aéronomie, Université Paris 6, Paris, France*

(Manuscript received 26 October 1998, in final form 21 April 1999)

ABSTRACT

Bidirectional polarized reflectances measured with the POLDER-1 instrument on board *Advanced Earth Observing Satellite-1* have been used to infer cloud altitude and thermodynamical phase (ice/liquid) at a global scale. This paper presents a validation of these properties for cirrus clouds. The validation presented here is based on comparisons between POLDER-1 retrievals and measurements collected with a ground-based lidar network. The scale differences between POLDER measurements and lidar data are treated by selecting homogeneous and stable cloud layers.

These comparisons show that the cloud altitude retrieval with POLDER is valid for optically thick cloud, and nonvalid for semitransparent and thin cirrus clouds. The limitations of the cloud altitude retrieval method are analyzed by using both comparisons between POLDER and lidar and simulations of the bidirectional polarized reflectances performed with a radiative transfer code to assess a threshold of validity of the POLDER retrieval method. The comparisons of lidar and POLDER data show that the cloud thermodynamical phase (ice/liquid) retrieval is satisfactory, and examples of cloud thermodynamical phase retrieval are presented as a function of cloud temperatures.

1. Introduction

The occurrence of cirrus clouds inferred from satellite data is usually larger than 50% at mid- and tropical latitudes. These high clouds have a major influence on the earth–atmosphere energy budget through a combination of factors including large coverage, both in space and time, and low temperature. They influence the energy balance through effects on incoming solar radiation and outgoing infrared radiation (Liou 1986). At the present time, the impact of cirrus clouds on climate change is accepted in a broad sense but still needs to be asserted more quantitatively (Hansen et al. 1984). Among the missing quantities are the key radiative properties, that is, optical depth and microphysical characteristics, as well as structural parameters, for example, height, geometrical thickness, and geographical coverage. The ice crystal size in cirrus cloud is variable, and the particle shape can be complex. In situ measurements can be used to observe cirrus cloud composition, but it requires high altitude aircraft because of the high altitude of cirrus clouds. In addition, semitransparency makes high clouds difficult to detect in satellite data and gives an inherent difficulty to discriminate between ice and liquid water.

At the present time, cloud parameters on a global scale are derived from observations by space-based radiometers (in sun-synchronous or geostationary orbit). Recently, the French space agency Centre National d'Études Spatiales developed a new radiometer, the POLDER (Polarization and Directionality of the Earth's Reflectances; Deschamps et al. 1994). POLDER was launched in August 1996 on board the Japanese heliosynchronous *Advanced Earth Observing Satellite-1* (*ADEOS-1*) (1030 LST) orbiting at 796-km altitude. The inclination is 98.59°, and the orbit period is 100 min.

POLDER-1 data inversion algorithms are currently under validation. As part of this ongoing effort, we focus our current research on cirrus clouds, with special attention paid to two parameters that can be inferred from polarized radiances: cloud height and discrimination between ice and liquid water (i.e., thermodynamical phase). The validation is conducted by comparison with contemporary lidar measurements. The current validation involves a lidar network of four ground-based stations distributed over different latitudes in the two hemi-

Corresponding author address: Dr. Hélène Chepfer, Laboratoire de Météorologie Dynamique, École Polytechnique, 91128 Palaiseau CEDEX, France.
E-mail: chepfer@lmd.polytechnique.fr

TABLE 1. POLDER cloud products deduced from polarized measurements.

Cloud parameter inferred from polarized data	Inversion method	POLDER-1 measurements
Height	Rayleigh pressure method (Goloub et al. 1994)	Bidirectional polarized reflectances at 443 and 864 nm
Thermodynamical phase	Absence or presence of rainbow $\Theta = 140°$ (Goloub et al. 1994)	Bidirectional polarized reflectances at 864 nm around $\Theta = 140°$
	Particle shape signature for scattering angles lower than 110°	Bidirectional polarized reflectances at 864 nm for scattering angles lower than 110°

spheres. Lidars can detect subvisible cirrus clouds, and they are well suited to retrieve cloud boundaries (height) with high accuracy (tens to hundred of meters) and properties such as the optical depth and backscattering phase function. This latter parameter provides information on the cloud particle microphysics, while lidar linear depolarization ratio (Sassen 1991) provides relevant information on cloud phase. Prior to the current work, POLDER radiometer data have been used in conjunction with backscatter lidar data in the framework of an airborne experiment (Sauvage et al. 1999; Chepfer et al. 1999).

Section 2 addresses the mean features and capabilities of POLDER-1 on *ADEOS-1*. Section 3 is dedicated to the POLDER data inversion techniques used to derive the cloud information to be validated. Section 4 presents the lidar network and lidar data. The implemented procedure to conduct a reliable comparison between POLDER-1 and lidar is discussed in section 5. Sections 6 and 7 present the results of the comparisons for cloud height and cloud phase, respectively.

2. POLDER radiometer on *ADEOS-1*

The POLDER instrument was designed to collect accurate observations of the polarized and directional solar radiation reflected by the earth–atmosphere system (Deschamps et al. 1994). The data collected by POLDER-1 are currently used to address several key scientific objectives related to climate change: 1) cloud climatology, or description, and earth radiative budget (Buriez et al. 1997), 2) atmospheric aerosols and earth radiative budget (Herman et al. 1997), 3) atmospheric water vapor amount and atmospheric branch of the hydrological cycle (Vesperini et al. 1999), 4) ground reflectances and surface cover change (Leroy et al. 1997), and 5) ocean color. Considering the most important cloud parameters relevant to the earth radiative budget, the polarization measurement capability of the new radiometer is used in the current paper to infer the height and thermodynamical phase of cirrus clouds. The first radiometer POLDER-1 was operational for 8 months, from 1 November 1996 to 30 June 1997. A follow-on POLDER-2 should be launched on *ADEOS-2* in the summer of 2000.

The POLDER instrument concept is based on a charged coupled device (CCD) matrix array detector, a rotating filter wheel, and wide field-of-view optics for both alongtrack and cross-track directions with a maximum field of view of 114° (Deschamps et al. 1994). The POLDER cross-track swath is about 2200 km, allowing for near-complete daily coverage of the earth. The CCD matrix is 242 × 74 pixels, with pixel resolution at nadir equaling 6 km × 7 km. An atmospheric target can be observed several times in different perspectives (14 at maximum). The viewing directions correspond to scattering angles between 70° and 180° depending on the solar zenith angle and ADEOS positioning with respect to the target.

The reflectance measurements are taken in eight different wavelengths bands: 443 (20), 490 (20), 565 (20), 670 (20), 763 (10), 765 (40), 865 (40), and 910 nm (20 nm), where the first number is the wavelength of the band center and the second one the bandwidth. Three of these channels, that is, 443, 670, and 865 nm, measure the state of polarization of the reflected solar radiation. The potential of polarization measurements for atmospheric applications was pointed out by Hansen (1971) and van de Hulst (1981), and more recently by Herman et al. (1997). The state of polarization of the scattered radiation is sensitive to the shape of the scatterers and is particularly relevant for the study of ice clouds. In this study we used the POLDER-1 measurements in the two polarized channels: 443 and 865 nm.

3. Inversion method for POLDER data

The POLDER cloud algorithms are presented in Buriez et al. (1997). The main output of the data inversion process are the (i) cloud-top height, (ii) cloud phase, and (iii) cloud optical depth (using an a priori microphysical model for a given cloud type). As stated before, the present study focuses on the validation of the quantities inferred from polarized radiance measurements, that is, cloud-top height using the so-called Rayleigh pressure method, and cloud phase (Table 1; Goloub et al. 1994).

The Rayleigh pressure method is based on an accurate determination of the integrated air column above a cloud using the polarized radiances at 443 and 864 nm. It relies on three basic properties: (i) the intensity of the Rayleigh scattering by molecules is a significant contribution at 443 nm, but it is weak at 864 nm; (ii) the scattered

intensity by ice crystals is about the same in the two channels, and (iii) the first orders of scattering provide the main contribution to POLDER polarized radiances.

Let us assume that the polarized light reflected by the cloud does not depend on the wavelength, because of the large dimension of the cloud droplets or ice crystals, and that the light resulting from multiple interactions between the cloud and the molecular layer exhibits negligible polarization. The expected polarized radiance L_p will be

$$L_p = L_{p,m} + L_{p,c} \exp\left[-\delta_m\left(\frac{1}{\cos\theta_s} + \frac{1}{\cos\theta_v}\right)\right], \quad (1)$$

where δ_m is the optical thickness of all molecules above the cloud, $L_{p,m}$ stands for the polarized light due to molecular scattering, and $L_{p,c}$ stands for the polarized light at the top of the cloud when directly illuminated by the solar beam; the exponential term accounts for the attenuation by the overlying molecular layer. To simplify (1), as δ_m and $L_{p,m}$ are negligible at $\lambda = 864$ nm, let us consider that L_p ($\lambda = 864$ nm) directly provides $L_{p,c}$, and let us neglect the transmission effect, which is justified for high-level clouds. Then, (1) reduces to

$$L_p^{443} - L_p^{864} \approx L_{p,m}^{443}. \quad (2)$$

Let $\delta_m(\lambda)$ be the optical thickness of the molecular layer; because $\delta_m(\lambda)$ is small, single scattering approximation of $L_{p,m}$ is valid in first approximation and therefore

$$L_{p,m}^{443} = \delta_{0,m}^{443}\left(\frac{p}{p_0}\right)\frac{p_m(\Theta)P_m(\Theta)}{\cos\theta_v}$$

$$= \left(\frac{p}{p_0}\right)\frac{3\delta_{0,m}^{443}(1 - \cos^2\Theta)}{16\cos\theta_v}, \quad (3)$$

where $\delta_{o,m}^{443}$ is the total Rayleigh optical thickness, and p_m and P_m are, respectively, the molecule's phase function and polarization ratio. Equation (3) shows that the polarized light is mainly governed by the scattering angle Θ. The cloud-top pressure and surface pressures are, respectively, p and p_0. As a consequence, the difference between 443 and 864 nm will account for the molecular contribution above the cloud. Following (3) the cloud-top pressure is

$$p = C\frac{\cos\theta_v}{(1 - \cos^2\Theta)}(L_p^{443} - L_p^{864}) \quad (4)$$

with the constant C equal to 2.45×10^4 hPa.

The retrieved pressure is the average of the values calculated for all scattering angles ranging between 80° and 120°. The single scattering approach used for the Rayleigh model should be enough for high-level cloud observations since in that case the molecular layer above the cloud is very thin.

Cloud thermodynamical phase is inferred from polarized radiation measurements at 864 nm. The molecular contribution to the scattered radiation is weaker in this channel when compared with other available channels. An underlying assumption is that the polarized reflectance at this wavelength is mainly due to cloud particles. Discrimination between ice particles and water droplets is based on sensitivity of the normalized polarized radiance to scatterer shape (Goloub et al. 1994; Mishchenko and Travis 1997; Chepfer et al. 1998) as displayed in Fig. 1. The polarized radiance L_p is defined as

$$L_p = \sqrt{Q^2 + U^2 + V^2}, \quad (5)$$

where Q, U, and V are the Stokes parameters at the top of the atmosphere. The normalized polarized radiance $L_{n,p} = \pi L_p/E_s$, where E_s is the incident light at the top of the atmosphere. The normalized polarized radiance $L_{n,p}$ is linked to the bidirectional polarized reflectance ρ_p as $\rho_p = L_{n,p}/\mu_s$. The polarized radiance $L_{n,p}$ at 864 nm reflected by a cloud composed of spherical particles or hexagonal plates randomly oriented in space has been simulated using an adding–doubling radiative transfer code (de Haan et al. 1986). The scattering matrices are computed using Mie theory for water droplets ($r_e = 20$ μm) and a ray-tracing code accounting for the Fraunhofer diffraction in the forward direction for ice crystals (aspect ratio $Q = 0.05$; $r_e = 20$ μm; Brogniez 1988; Chepfer 1997). In Fig. 1, the scattering angles range from 70° to 175°, the limited number of cross (ice plates) and dot (spheres) points represent each POLDER observation (11 in the current case), the solar zenith angle $\theta_s = 55°$, and cloud optical depth $\delta = 2$.

Figure 1 shows two ranges of scattering angles suitable to discriminate between ice and liquid water: (i) between 130° and 140°, where a strong peak corresponds to the rainbow phenomena for liquid water cloud, and the normalized polarized radiance displays a smooth behavior for ice plates; and (ii) between 70° and 120° where the slopes are quite different—positive for droplets and negative for ice plates. The sensitivity of the polarized radiance to the crystal habit (hexagonal plates, columns, polycrystals, etc.) has been studied in Chepfer et al. (1998). In practice, the information contained in the two scattering angle ranges are complementary, since normally POLDER cannot observe the full range of scattering angles depending on the respective orientations of the sun and satellite track. In practice, the use of any of these two ranges of scattering angles can discriminate the cloud thermodynamical phase for most of the actual POLDER viewing geometry.

4. Lidar network and dataset

The current validation of cirrus cloud-top height and thermodynamical phase takes advantage of lidar measurements conducted at different sites during the POLDER-1 operational phase.

a. The lidar network

The ground-based lidar network involves four geographically diverse sites: two are located in the Northern

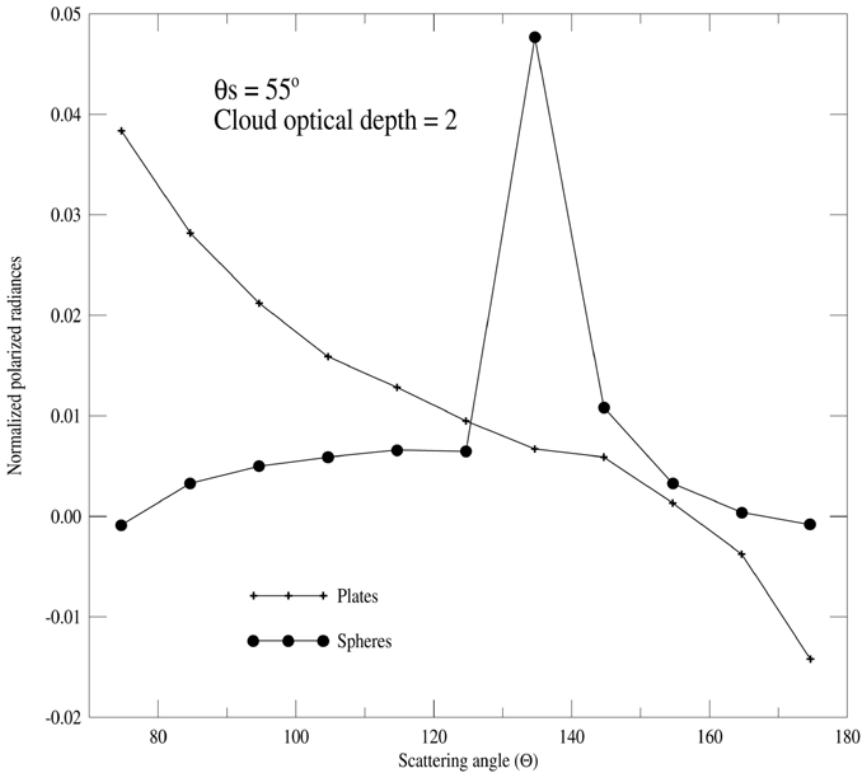

FIG. 1. Bidirectional polarized radiances simulated for a water cloud composed of spherical particles (large dot), and for an ice cloud composed of nonspherical particles (cross). The bidirectional polarized radiances are plotted as a function of the scattering angle.

Hemisphere, and two are in the Southern Hemisphere. The characteristics of the different sites and the parameters of the lidar systems are presented in Table 2. Two of them are devoted to research activities (Palaiseau, Buenos Aires) and are operated at the convenience of the experimenters for the purpose of research work, whereas the other two are new micropulse (MP) lidar systems (Spinhirne et al. 1995). The MP lidar systems operate hands-off and continuously at currently two U.S. Department of Energy Atmospheric Radiation Measurement (ARM) sites in central Oklahoma and Manus Island, Papua New Guinea. The four lidars probe the atmosphere in the visible at approximately the same wavelengths: 532 and 523 nm. The time resolution is better for research lidar than for the MP lidar for which 1-min signal integrations are recorded. In addition, these lidars can penetrate thicker clouds, and one of them has depolarization capability to discriminate between spherical and nonspherical particles. In most cases the lidar depolarization ratio $\Delta = S_p/S_s$ is larger than 0.2 in cirrus clouds, where S_p and S_s are the lidar signals with perpendicular and parallel polarizations, respectively (Sassen 1991).

TABLE 2. Lidar sites and characteristics of four ground-based lidar systems.

	Palaiseau, France	Oklahoma	Manus Island, Papua New Guinea	Buenos Aires, Argentina
Lat	48.43°N	36.61°N	2.06°S	34.60°S
Long	2.15°E	97.41°W	147.44°W	58.50°W
Altitude	115 m	315 m	5 m	0 m
Environment	Continental suburban	Continental Great Plains	Pacific Ocean	Coastal Urban
Lidar type	Research	Micropulse lidar	Micropulse lidar	Research
Wavelength	0.532 μm	0.523 μm	0.523 μm	0.532 μm
Energy per pulse	150 mJ	10 μJ	10 μJ	200 mJ
Divergence	0.3 mrad	0.1 mrad	0.1 mrad	0.3 mrad
PRF	20 Hz	2500 Hz	2500 Hz	10 Hz
Receiver diameter	60 cm	20 cm	20 cm	50 cm
Field of view	2 mrad	0.1 mrad	0.1 mrad	2 mrad
Depolarization capability	Yes	No	No	No
Institution	LMD	ARM	ARM	CEILAP

TABLE 3. Cases selected for validation.

	Palaiseau, France	Oklahoma	Manus Island, Papua New Guinea	Buenos Aires, Argentina
Period of observation	Feb 1997–Jun 1997	Oct 1996–Jun 1997	Apr 1997	Nov 1996–Jan 1997
ADEOS overpass	1000–1100 UTC	1700–1800 UTC	1900–2000 UTC	1400–1500 UTC
No. of cases	6	140	9	1
Single semitransparent cirrus layer	2	21	1	1
Single thick cirrus layer	0	8	1	0
Low-level cloud	4	111	7	0

The different sites include a radiosonde capability and others remote sensors. In the current study the temperature profiles are used to complement the lidar measurements in order to derive the cloud phase (see section 7).

The distribution of the four ground-based lidar stations in the two hemispheres and in different latitude bands allows for some account of the natural geographical variability of cirrus clouds. The optical and structural properties depend on the conditions of formation and maintenance, which in turn depend very much on key meteorological variables, for example, temperature, humidity, wind shear, and seeding by icing cloud nuclei [Sassen et al. 1995; see the special section Subsonic Aircraft: Contrail and Cloud Effects Special Study (SUCCESS 2), in *Geophysical Research Letters*, 1998, Vol. 25, No. 10].

b. Selected cases for validation

The entire lidar network collected 259 periods of observations coinciding with POLDER-1 overpasses (see section 5) from 1 November 1996 until 30 June 1997. From this sample, final case selection for validation purposes was conducted according to the following criteria: (i) the lidar measurements were performed during at least 1 h before and after ($\pm$1 h) the satellite ADEOS overpass time, and (ii) multilayers (i.e., occurrence of broken low clouds and high clouds) and highly heterogeneous cirrus clouds were not considered.

The total number of cases selected for validation at each site varies in large proportion, between operational and research sites, with the ARM sites providing the bulk of the 49 cases out of 156 ultimately used. The cases are divided into three categories: (i) single semitransparent cirrus cloud layer that can be penetrated by any lidar in order to retrieve the cloud boundaries (cloud base and top) at the same time (i.e., an approximate signal-to-noise ratio SNR $>$ 3 at cloud top), (ii) single thick high layers such that only the cloud base can be observed by lidar, and (iii) mid- and low-level clouds. Table 3 summarizes the results of the selection process.

c. Inversion methods for lidar data

The lidar measurements collected at the different sites were each processed identically as follows.

1) We develop our own algorithm to retrieve the cloud boundaries from the range-corrected lidar signal, that is, $R^2S(R)$, where R is the lidar range and S the total lidar signal, using thresholding sets at $SNR > 3$. The cloud-top and -base altitude uncertainty is $\pm$30 m for the research lidars and $\pm$150 m for the MP lidars. (Standard MP lidar cloud boundary data are also available from the open ARM data system but do not currently identify the true cloud top.)
2) The cloud phase is assessed from cloud-height and temperature profiles recorded by radiosonde. We considered the formation of ice clouds to occur at temperatures less than -40°C. In addition, we used the lidar depolarization ratio (Δ) for measurements collected in Palaiseau.
3) The cloud optical depth estimations are obtained in four steps as follow: 1) the lidar signals are normalized to the backscatter signal from molecules assuming a scattering ratio equal to 1.1 or less in clear zones above and/or below the cirrus cloud deck, 2) a mean backscatter-to-extinction ratio k is derived from at least six time samples every 10 to 15 min (Young 1995), 3) a forward solution of the lidar equation allows for determination of a vertical profile of apparent extinction coefficient (Fernald et al. 1972) α_a and so an apparent optical depth δ_a, and 4) this apparent optical depth is corrected for multiple scattering for research lidars; the true optical depth is $\delta = 2\delta_a$ (Nicolas et al. 1997). The correction does not apply to MP lidar data, for they operate with a narrow field-of-view transceiver (see Table 2). The overall uncertainty in optical depth is on the order of 20%–30%. In the case of thick cirrus clouds, when the cloud top cannot be detected in a reliable way, the optical depth is given a minimum value $\delta = 1.5$ for MP lidars and $\delta = 3$ for research lidars (thanks to the multiple scattering effects). It correspond to a minimum measurable value of $T^2 = 0.05$.

5. Implemented procedure for validation

At present, the comparison bears on cloud-middle height and cloud phase for the cirrus cloud cases selected according to section 4. A major source of uncertainty and discrepancy may come from different footprints for POLDER-1 and ground-based lidars. POLDER horizontal resolution for a single pixel is about 6 km $\times$ 7 km at nadir whereas the lidar beam at cirrus cloud level is several meters or tens of meters depending

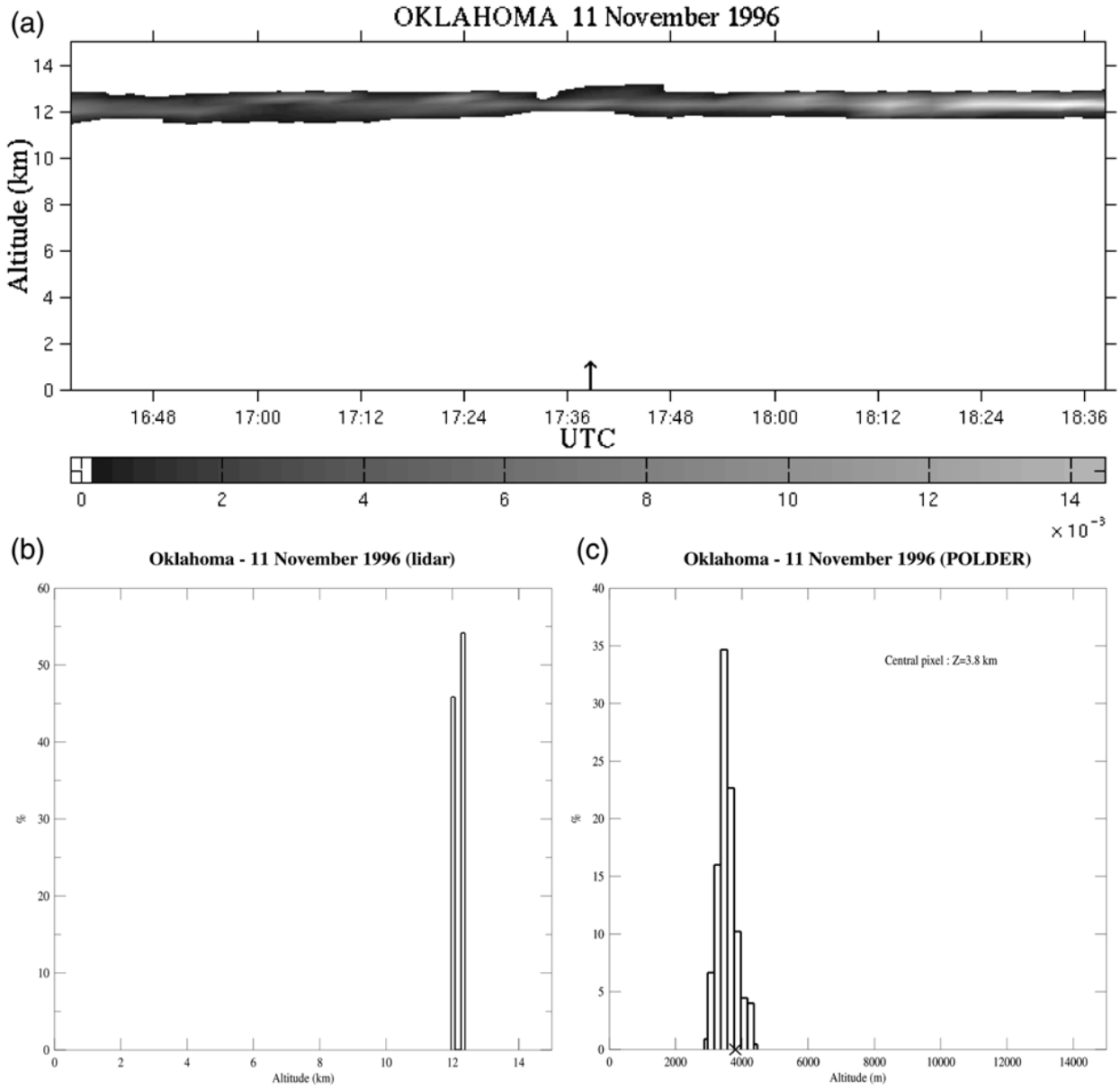

FIG. 2. Cloud altitude for 11 Nov 1996 at the Oklahoma CART site. (a) Cloud altitude deduced from lidar measurements as a function of time. (b) Histogram of cloud altitude inferred from lidar measurements. (c) Histogram of cloud altitude inferred from POLDER data in an area of 15 × 15 pixels around the lidar site.

on the system. In order to account for such a difference in footprint we proceeded in two steps. (i) First, we take the cloud-top height and cloud phase computed for a single POLDER pixel corresponding to lidar site and compare with the lidar values at the time of satellite overpass. (ii) Second, we compare the POLDER information in a 15 × 15 (or 125 total) pixel area (at least 100 km × 100 km at nadir, and more in other configurations) to the values derived by lidar during a 2-h time period (±1 h) about the time of satellite overpass.

If the lidar time series show a strong variability or when the POLDER-1 histogram indicates a highly dispersed dataset, then the cloud case is not accounted for in the final result.

6. Results for cirrus cloud altitude

a. Selected examples

Figure 2 shows a comparison between a lidar time series recorded at the Oklahoma Cloud and Radiation Testbed (CART) site on 11 November 1996 (panel a) and lidar histogram for cloud middle height (panel b), with a POLDER-1 histogram for cloud height (panel c).

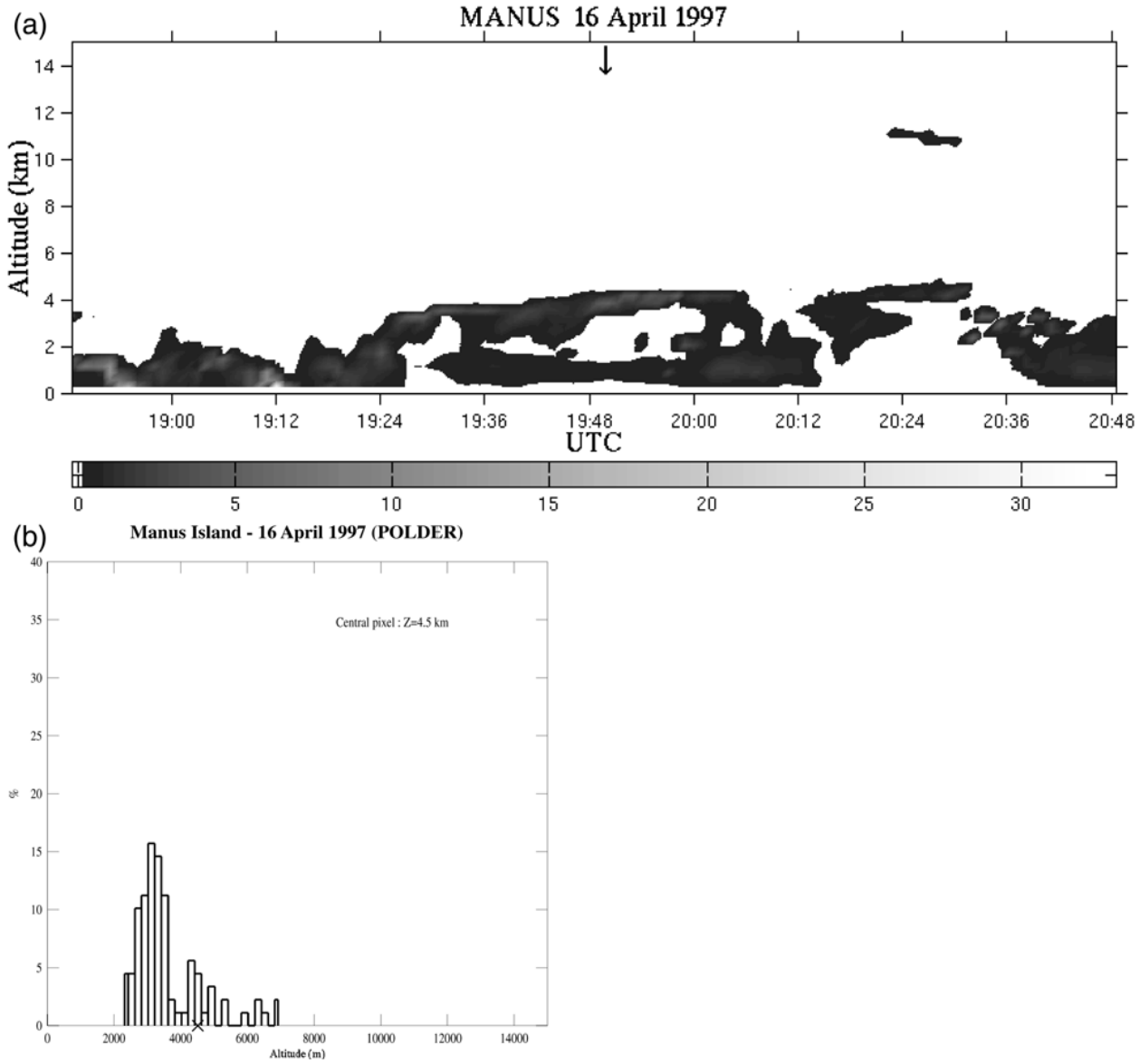

FIG. 3. Cloud altitude for 16 Apr 1997 at the Manus Island site. (a) Cloud altitude deduced from lidar measurements as a function of time. (b) Histogram of cloud altitude inferred from POLDER data in an area of 15 × 15 pixels around the lidar site.

The time of POLDER-1 overpass, 1738 UTC, is indicated by a vertical arrow in Fig. 2a. The height assigned on the POLDER-1 pixel matching the lidar site is 3.8 km, and it is marked by a cross in Fig. 2c. The cloud height derived from POLDER-1 data makes use of the Rayleigh pressure method (see section 3). The lidar time series shows a single cirrus cloud layer between 11- and 13-km altitude. The layer is stable during two hours as required for a reliable validation (see section 5). The large difference in height may be due to a small optical depth as indicated by lidar measurements ($\delta = 0.2$ at 1738 UTC) (see discussion in section 6c).

Figure 3 shows a comparison from Manus Island data on 16 April 1997. The low-level cloud cannot fully transmit the lidar beam, and the highest cloud layer seen is 4-km altitude (Fig. 3a). POLDER-1 overpassed Manus Island at 1949 UTC. The altitude inferred from POLDER data using the Rayleigh pressure method (presented in Fig. 3b) ranges between 2.5 and 7 km. The height assigned on the POLDER-1 pixel matching the lidar site is 4.5 km; it is marked by a cross in Fig. 3b. The pixels associated with the highest values of altitude correspond to cloud layers that cannot be detected by the laser beam. From lidar analysis, the cloud optical depth is higher than 1.5.

Figure 4 shows a comparison conducted for data from Oklahoma on 26 January 1997. The cloud bottom is located at 6-km altitude as measured by lidar (Fig. 4a). The MP lidar cannot penetrate such a thick cloud so the cloud top is not determined. POLDER-1 overpassed

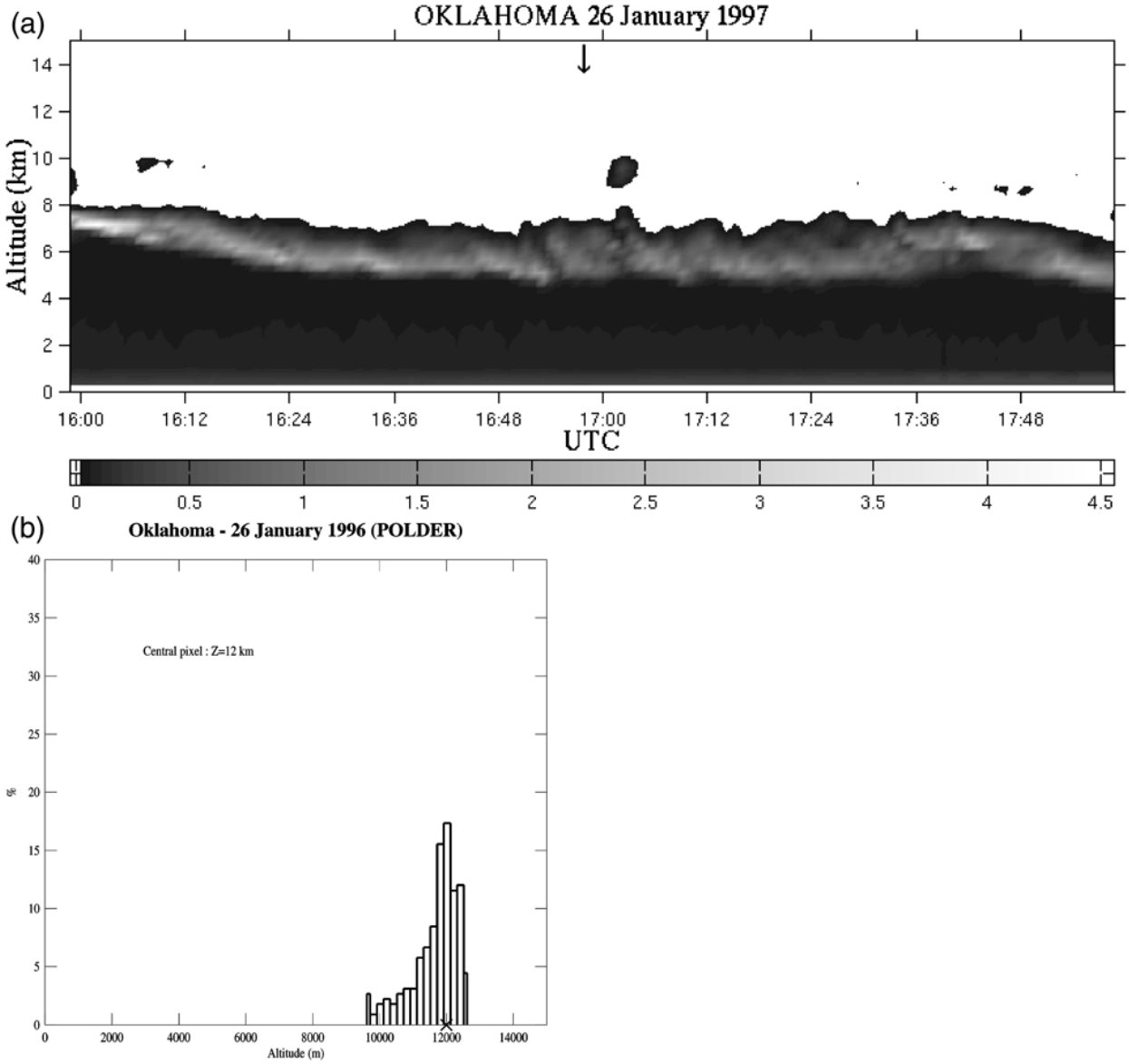

FIG. 4. Cloud altitude for 26 Jan 1997 at the Oklahoma CART site. (a) Cloud altitude deduced from lidar measurements as a function of time. (b) Histogram of cloud altitude inferred from POLDER data in an area of 15 × 15 pixels around the lidar site.

Oklahoma at 1659 UTC. The altitude inferred from POLDER data using the Rayleigh pressure method is presented in Fig. 4b; it ranges between 10 and 12 km. In this case POLDER-1 provides a cloud altitude higher than the one indicated by the lidar. The difference is due to the presence of an optically thick low-level cloud through which the laser beam cannot pass; hence, the lidar does not see the higher cloud layers detected with POLDER.

b. Analysis of 34 cases

A total of 34 cases of cirrus cloud have been analyzed following the methodology presented above. The height difference between the cloud-middle altitude measured by lidar and the cloud height inferred from the POLDER-1 data on the pixel corresponding to the lidar site is plotted in Fig. 5 as a function of cloud optical depth derived from lidar measurements. When the lidar cannot reach the cloud top the cloud optical depth has been set equal to 1.5 for MP lidars. No measurements on thick cirrus cloud taken by research lidars have been used so far for the validation. Figure 5 clearly shows that the lower the cloud optical depth the bigger the bias is. POLDER underestimates the cloud height for low optical depth while the lidar may underestimate the height for large optical depth when POLDER makes a fair estimate.

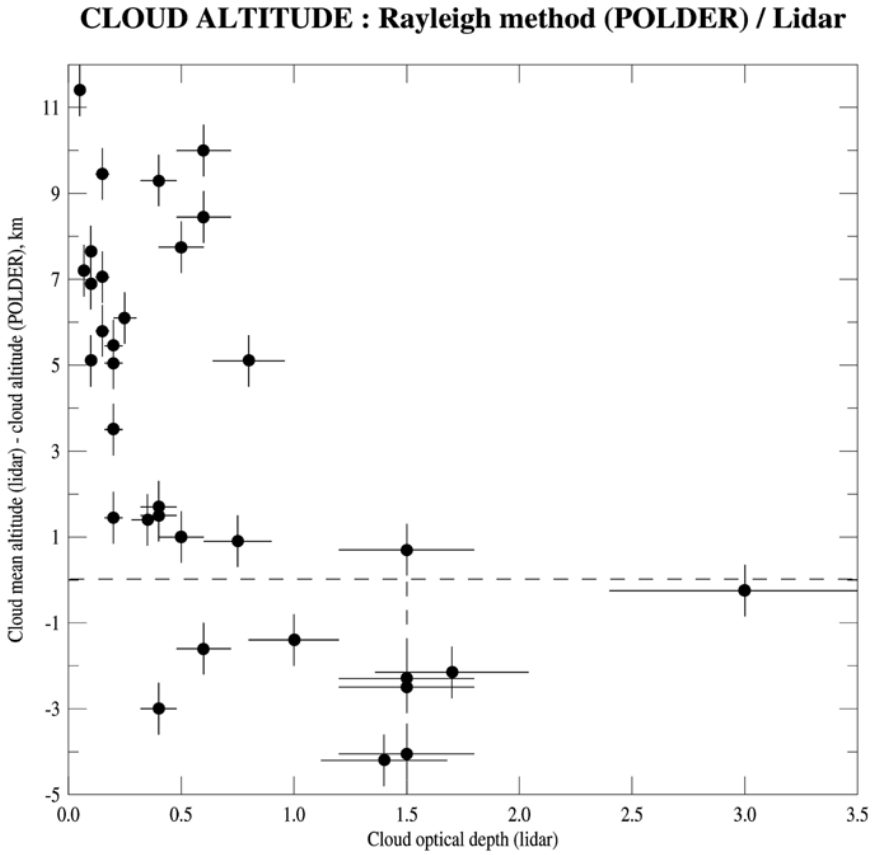

FIG. 5. Differences between cloud altitude inferred from POLDER and cloud-mean altitude measured with lidar as a function of the lidar cloud optical depth. Error bars correspond to the uncertainty on the lidar optical depth (±20%), and to the sum of uncertainties on lidar and POLDER cloud-top altitudes.

c. Discussion of the results

In order to understand the possible limitation of the Rayleigh pressure method used in POLDER inversion to infer cirrus cloud height, it was applied to simulated POLDER polarized radiances at 443 and 864 nm for a prescribed atmosphere. The polarized radiances at the top of the atmosphere are calculated using an adding–doubling code (de Haan et al. 1986). The atmosphere is composed of three layers: (i) air molecules between the surface and 400 hPa, (ii) air molecules and ice particles between 300 and 400 hPa, and (iii) air molecules above 300 hPa. We considered two different types of ice particles: hexagonal plates and polycrystals. A ray tracing code accounting for Fraunhofer diffraction in the forward direction is used to compute the scattering matrix of hexagonal plates (Brogniez 1988; Chepfer 1997), while the scattering matrix for polycrystals is taken from Macke et al. (1996).

The simulations were conducted for different optical depths and various solar zenith angles. Figure 6a displays the retrieved cloud height in pressure units as a function of cloud optical depth, considering a solar zenith angle $\theta_s = 30°$ for plates (solid line), and for polycrystals $\theta_s = 30°$ (dashed line with open circle) and $\theta_s = 60°$ (dashed line with cross). In all cases the POLDER polarized radiances are simulated in the principal solar plane for a relative azimuth angle $\Delta\Phi = 0$ (where $\Delta\Phi = \Phi_s - \Phi_v$; Φ_s, and Φ_v are, respectively, the azimuth solar angle and the azimuth viewing angle). Figure 6a shows that the height is underestimated for moderate optical depth as the bias is nearly zero when $\delta > 1.5$–3 for cloud-base height, and when $\delta > 3$–4 for cloud-top height, depending on the crystal types and experimental conditions. The sensitivity to ice particle shape is more than 100 hPa for solar zenith angle of 30°. The bias is larger at small solar angle for which the transmission is comparatively larger.

Figures 6b and 6c display the cirrus cloud height as a function of $\Delta\Phi$ with values ranging from 0° to 80°. The simulations are conducted for two values of the optical depth equal to 1 (Fig. 6b) and 4 (Fig. 6c), for the two ice crystal shapes used above and the same solar angles. Those figures show that the restitution of the cloud pressure using the Rayleigh pressure method is weakly sensitive to the azimuth viewing angle of POLDER. Figure 6b shows that the results and bias do not

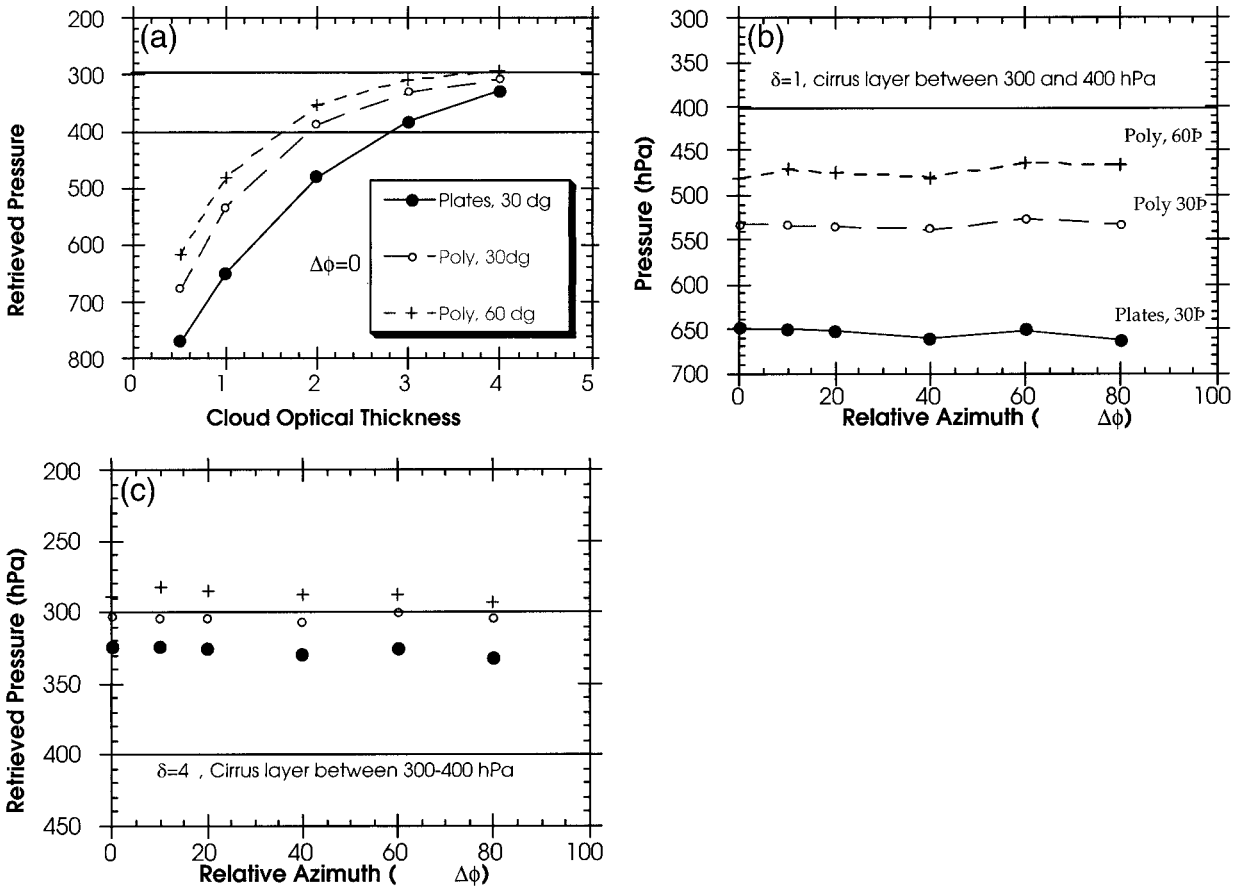

FIG. 6. (a) Simulations of the difference between the altitude of a cloud and the altitude deduced from the polarized bidirectional reflectances in the solar principal plane, as a function of the cloud optical depth for a solar zenith angle $\theta_s = 60°$, and a solar zenith angle $\theta_s = 30°$. Simulations of the cloud pressure retrieved with the Rayleigh pressure method for a cirrus cloud located between 300 and 400 HPa, with an optical depth of (b) $\delta = 1$ and (c) $\delta = 4$, respectively, as a function of the relative azimuth angle ($\Delta\Phi$).

depend on the relative azimuth angle, but rather on the crystal types and solar angle. Figure 6c shows a fair agreement between the input and outputs of the simulation for thick optical depth.

A conclusion drawn from these results is that the Rayleigh pressure method cannot be used for cirrus clouds as it stands and needs to account for actual optical depth. However, a threshold can be set for a reliable application of the method for cloud-top retrieval by considering Figs. 6a and 6b. For cirrus clouds composed of hexagonal plates with an optical depth larger than 4 or for cirrus cloud composed of polycrystals with an optical depth larger than 3, these values correspond to a hemispherical reflectance of 30%. At a later stage, the POLDER algorithm could be improved by an empirical correction accounting for the solar angle and hemispherical reflectance measured by POLDER.

7. Results for cloud phase

The cloud phase inferred from the POLDER-1 polarized radiances is compared with the cloud temperature assessed by radiosonde and lidar, assuming that only ice particles are present for temperatures lower than −40°C. This threshold value is considered safe for all meteorological conditions. Clouds located at temperature ranging between −20° and −40°C can be of mixed-phase with liquid and ice particles. We derived the cloud thermodynamical phase inferred from POLDER in a 3 × 3 pixel (or 20 km × 20 km) area around the lidar site for three ranges of cloud temperatures (i) $T <$ −40°C, (ii) −40°C $< T <$ −20°C, and (iii) −20°C $< T$.

a. Selected examples

Figure 7 shows the cloud boundaries derived by lidar and the corresponding temperature range for the case of 28 February observed at Palaiseau. The cloud is located between 9- and 12-km altitude as measured with the lidar (Fig. 7a). ADEOS overpassed Palaiseau at 1026 UTC. The cloud temperature ranges between −45° to −68°C (Fig. 7b). The cloud phase is ice as inferred from an area of 3 × 3 POLDER-1 pixels around the site. Figure 8 shows a similar example observed at the same

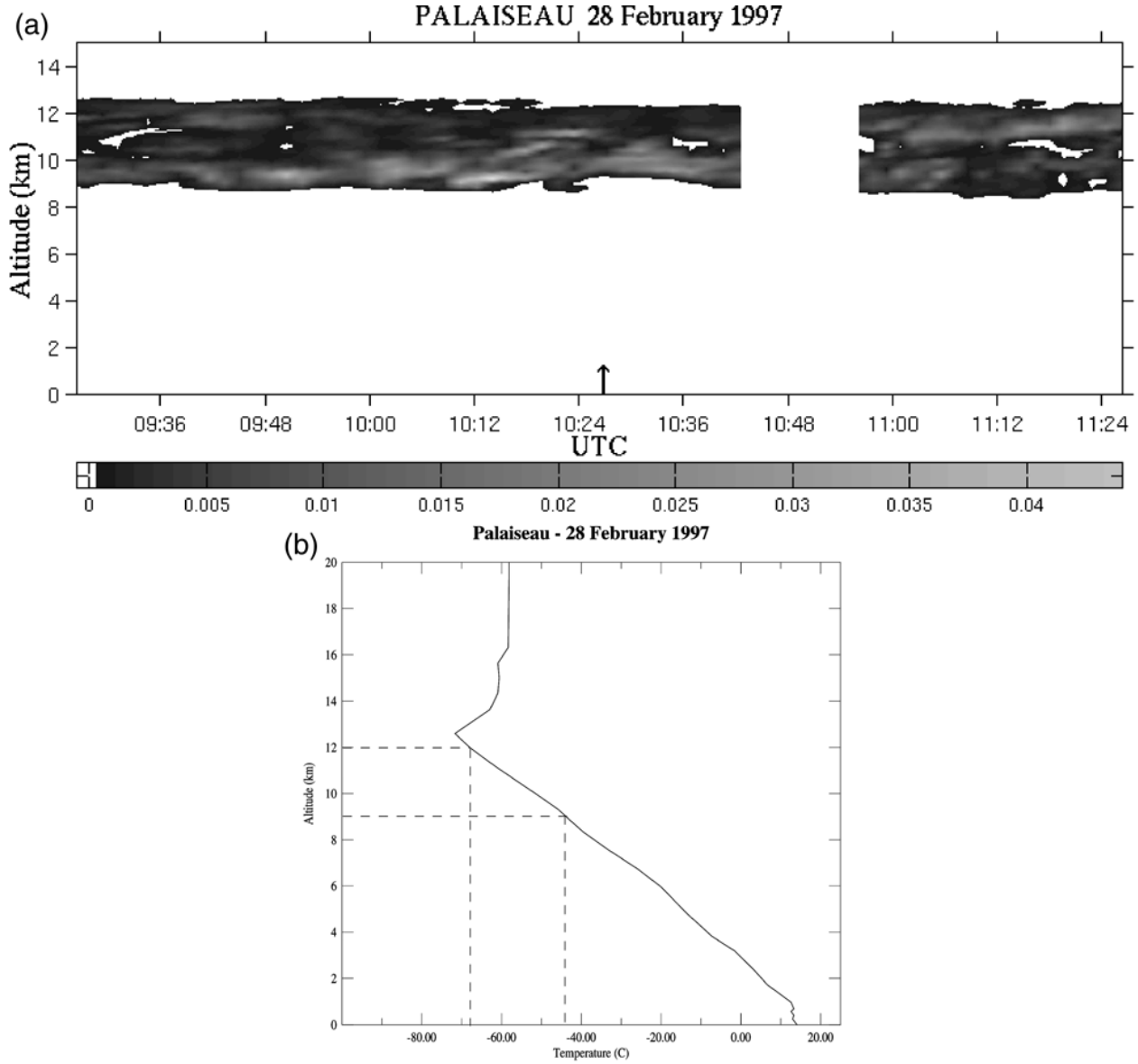

FIG. 7. (a) Lidar signal measured on 28 Feb 1997 at Palaiseau as a function of time. (b) Temperature profile in the atmosphere obtained with radiosonde.

location on 4 June 1997. The cloud is located between 8.5 and 11.8 km as measured with the lidar (Fig. 8a). ADEOS passed over Palaiseau at 1051 UTC. The cloud temperature ranges between −42° and −64°C (Fig. 8b) and the cloud phase is ice as inferred from and area of 3 × 3 POLDER-1 pixels around the site. Figure 9 shows an example observed at Manus Island on 18 April 1997. The cloud altitude ranges between 6 and 10 km (Fig. 9a). ADEOS overpassed Manus Island at 2049 UTC. The cloud temperature varies between −5° and −32°C, and the cloud phase is liquid as inferred from an area of 3 × 3 POLDER-1 pixels around the site. Figure 10 presents a cloud observed on 6 December 1996 in Oklahoma. The cloud sample consists of two layers ranging from 6 to 12 km (Fig. 10a). ADEOS overpassed the Oklahoma site at 1807 UTC. Cloud temperatures range between −18° and −65°C and cloud phase is mixed liquid and ice as inferred from an area of 3 × 3 POLDER-1 pixels around Oklahoma (seven pixels are identified as ice and two pixels as liquid phase).

b. Analysis of 32 cases

In order to conduct a reliable validation of cirrus cloud thermodynamical phase by POLDER-1 we selected cases where no low clouds were present in the lidar time series, and where the temperature at the cloud lower boundary is lower than −40°C. Accordingly, only

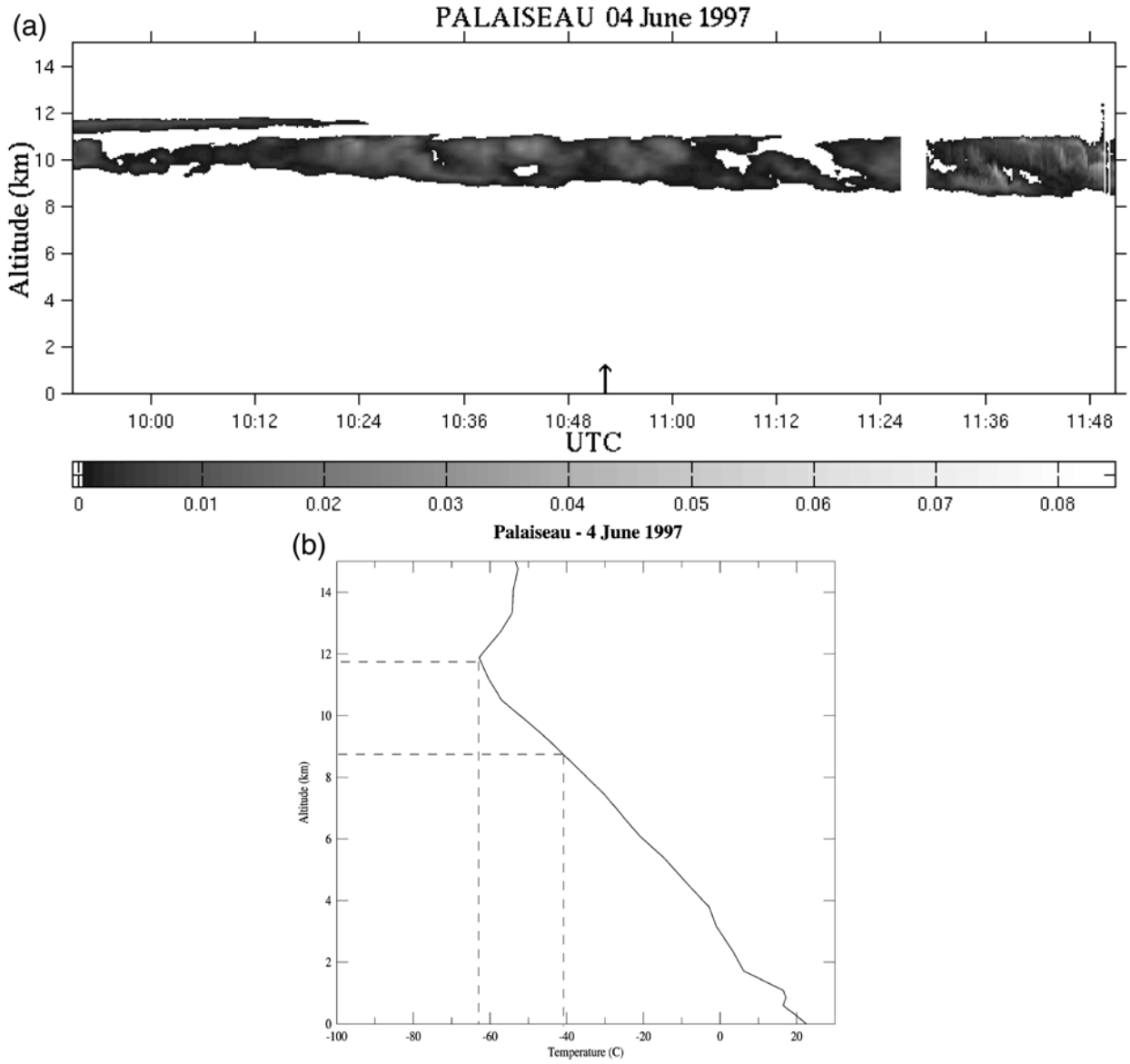

FIG. 8. (a) Lidar signal measured on 4 Jun 1997 at Palaiseau as a function of time. (b) Temperature profile in the atmosphere obtained with radiosonde.

32 cases out of the possible 150 are used in these study where 30 out of 32 are identified as ice (in all nine pixels) by POLDER and two as mixed clouds (ice and liquid water). Ice or liquid water means that all nine pixels identify ice or liquid water, respectively, while a mixed cloud is concluded when a single pixel contains information different from the others. The results are summarized in the first column of Table 4. For high clouds, the discrepancy is 6%.

c. Preliminary climatology derived from POLDER-1

The reliability of the present methodology is illustrated by the various examples presented in Figs. 7, 8, 9, and 10, and the results of the comparison for high clouds, which give a percentage of discrepancy of 6%, even if our dataset is limited at present. Since we are interested in a cloud global climatology emphasizing ice/liquid water discrimination, we derive such a climatology using all 150 cases. The results are presented in Table 4. The cloud thermodynamical phase determination with POLDER concerns mainly the higher layers of the cloud, whereas the cloud altitude observed with the lidar mainly detects the cloud base (when the cloud layer is thick or multiple). Nevertheless this preliminary climatology is consistent with other cloud thermodynamical phase determinations inferred from lidar measurements (Sassen et al. 1998; Sassen 1991; Sassen

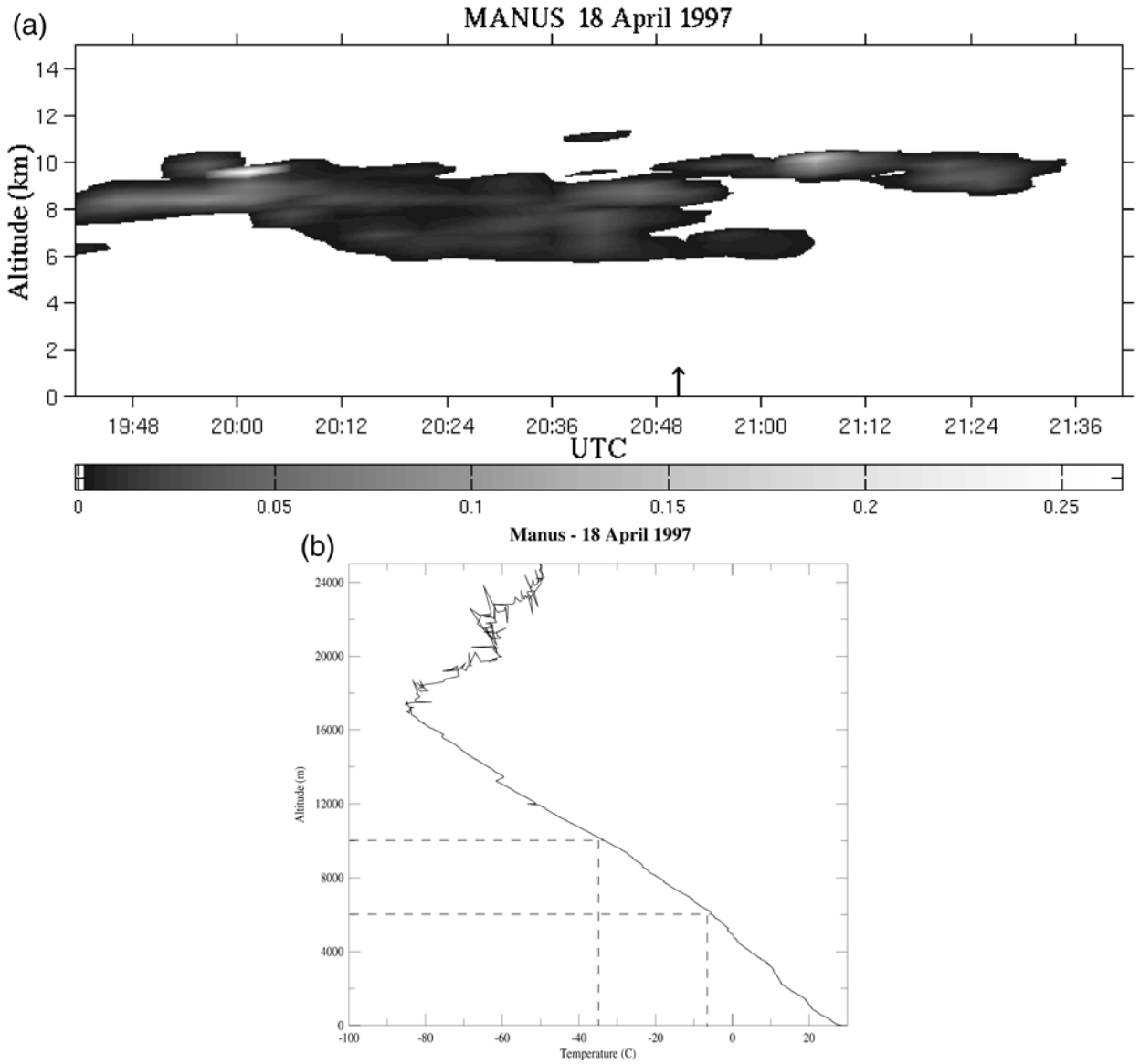

FIG. 9. (a) Lidar signal measured on 18 Apr 1997 at the Manus Island site as a function of time. (b) Temperature profile in the atmosphere obtained with radiosonde.

et al. 1979a,b) or in situ observations collected during intensive field experiments such as First International Satellite Cloud Climatology Project (ISCCP) Regional Experiment (FIRE) I and II (see special issues in Monthly Weather Review, 1990, Vol. 118, No. 11 and *Journal of the Atmospheric Sciences*, 1992, Vol. 52, No. 23) and SUCCESS 2.

8. Conclusions and future work

The main purpose of the current study was to conduct a validation of cirrus clouds parameters, that is, height and thermodynamical phase inferred from polarized POLDER-1 data collected from 1 November 1996 until 30 June 1997. The validation makes use of four ground-based lidar systems geographically distributed in latitude. The validation calls for cloud altitude as measured by lidar and temperature profile by the radiosonde. The methodology proposed is robust and reliable because range measurements by lidar are accurate and reliable. The cloud phase has been assessed using a temperature criterion in which presence of ice is asserted as certain for $T < -40°C$.

A validation of cloud height inferred from POLDER-1 using the so-called Rayleigh method has been conducted for 34 cases. It is shown that POLDER underestimates the cloud height for low values of cloud optical depth. A simulation confirms this result; it has been shown that a fair agreement is obtained when the optical depth is larger than 3, depending on crystal shape and experi-

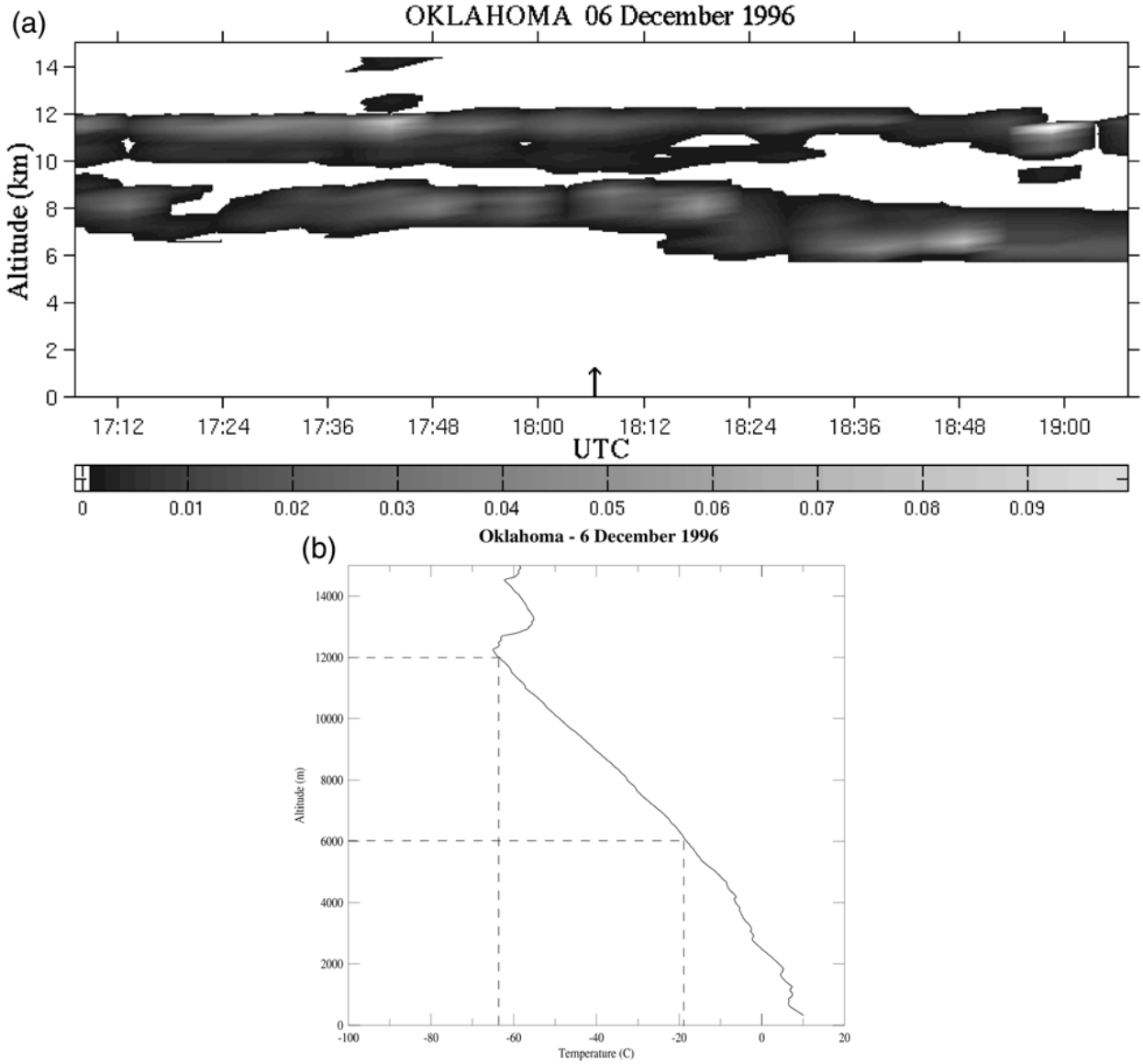

FIG. 10. (a) Lidar signal measured on 6 Dec 1996 at the Oklahoma CART site as a function of time. (b) Temperature profile in the atmosphere obtained with radiosonde.

TABLE 4. Cloud thermodynamical phase derived from POLDER-1 as a function of cloud temperature obtained from radiosonde data and collocated lidar height assignment. The cloud temperature is divided into three bins for temperature ranging from below −40°C, between −40° and −20°C, and above −20°C; the cloud thermodynamical phase is divided into three categories as ice only, mixed phase or ice and liquid water, and liquid water only. A total of 150 cirrus cloud cases have been selected and analyzed.

Cloud thermodynamical phase	$T <$ −40°C	−40°C $< T <$ −20°C	$T >$ −20°C	Total
Ice	30	22	28	80
Mixed phase	2	8	15	25
Liquid water	0	3	43	45
Total	32	32	86	150

mental condition (i.e., solar angle). Comparisons between POLDER-1 and lidar measurements, and simulations allow us to conclude that the Rayleigh pressure method is satisfactory only for thick clouds. Simulations show that it corresponds to cloud with hemispherical reflectances higher than 30%. In the near future, the Rayleigh pressure method could be improved for thin cirrus clouds using an empirical correction based on radiative transfer calculations, accounting for actual solar angle and hemispherical reflectance measured directly by POLDER. The cloud phase inferred from POLDER-1 data has been compared with the prediction of a combination of temperature and lidar measurements. A validation conducted on 32 cases shows a good agreement.

The current validation relying on a lidar network

could be implemented in the near future for the validation of sensors in the framework of the National Aeronautics and Space Administration Earth Observing Satellite program, and for POLDER-2 to be launched on the *ADEOS-2* satellite in the summer of 2000. It is anticipated that the MP lidar network will be expanded and more research lidar systems could be involved. It is therefore realistic that a total of 20 lidar systems could be involved in a validation effort covering the two hemispheres and all latitude bands.

Starting from the current validation for the cloud phase, future work could be directed to the establishment of a large-scale climatology of particle shape and preferred orientation of ice particles. The sensitivity of polarization measurements to the shape of scatterers will be investigated further to estimate the ice particle shapes. In addition, the bidirectional polarized reflectances will be used to assess a possible preferred horizontal orientation of ice crystals in cirrus clouds.

Acknowledgments. The authors are very grateful to J. Hovenier and J. de Haan from the Free University of Amsterdam who gave us the opportunity to use their doubling–adding radiative transfer code. Thanks are also due to A. Macke for providing us with the polycrystals scattering matrix. This study has been supported by Centre National d'Études Spatiales (CNES). The results presented here were obtained using a subset of the overall dataset collected by the CNES's POLDER radiometer on board the NASDA's ADEOS. The authors are very grateful to J.-M. Nicolas for the extraction of the useful POLDER data, and to J. Riedi for his participation in the analysis of POLDER cloud thermodynamical phase.

REFERENCES

Brogniez, G., 1988: Light scattering by finite hexagonal crystals arbitrarily oriented in space. *Proc. Int. Radiation Symp.*, Lille, France, International Association of Meteorology and Atmospheric Physics, 64–67.

Buriez, J. C., and Coauthors, 1997: Cloud detection and derivation of cloud properties from POLDER. *Int. J. Remote. Sens.*, **18,** 2785–2813.

Chepfer, H., 1997: Etude théorique et expérimentale des propriétés optiques et radiatives des cirrus. Ph.D. dissertation, Université de Lille-1, 197 pp.

——, G. Brogniez, and Y. Fouquart, 1998: Cirrus cloud microphysical properties deduced from POLDER observations. *J. Quant. Spectros. Radiat. Transfer*, **30,** 375–390.

——, ——, L. Sauvage, P. H. Flamant, V. Trouillet, and J. Pelon, 1999: Remote sensing of cirrus radiative parameters during EUCREX'94. Case study of 17 April 1994. Part II: Microphysical models. *Mon. Wea. Rev.*, **127,** 504–519.

de Haan, J. F., P. B. Bosma, and J. W. Hovenier, 1986: The adding method for multiple scattering calculations of polarized light. *Astron. Astrophys.*, **183,** 371–391.

Deschamps, P.-Y., F.-M. Bréon, M. Leroy, A. Podaire, A. Brickaud, J.-C. Buriez, and G. Sèze, 1994: The POLDER mission: Instrument characteristics and scientific objectives. *IEEE Trans. Geosci. Remote Sens.*, **32,** 598–615.

Fernald, F. G., B. M. Herman, and J. A. Reagan, 1972: Determination of aerosol height distributions by lidar. *J. Appl. Meteor.*, **11,** 482–489.

Goloub, P., J. L. Deuzé, M. Herman, and Y. Fouquart, 1994: Analysis of the POLDER polarization measurements performed over cloud covers. *IEEE Trans. Geosci. Remote Sens.*, **32,** 78–88.

Hansen, J. E., 1971: Multiple scattering of polarized light in planetary atmospheres. Part I. The doubling method. *J. Atmos. Sci.*, **28,** 120–125.

——, A. Lacis, D. Rind, G. Russel, P. Stone, I. Fung, R. Ruedy, and J. Lerner, 1984: Climate sensitivity: Analysis of feedback mechanisms. *Climate Processes and Climate Sensitivity, Geophys. Monogr.*, No. 29, Amer. Geophys. Union, 130–163.

Herman, M., J. L. Deuzé, C. Devaux, P. Goloub, F. M. Bréon, and D. Tanré, 1997: Remote sensing of aerosols over land surfaces, including polarization measurements: Application to some airborne POLDER measurements. *J. Geophys. Res.*, **102,** 17 039–17 049.

Leroy, M., and Coauthors, 1997: Retrieval of atmospheric properties and surface bidirectional reflectances over land from POLDER. *J. Geophys. Res.*, **102,** 17 023–17 037.

Liou, K. N., 1986: Influence of cirrus clouds on weather and climate processes: A global perspective. *Mon. Wea. Rev.*, **114,** 1167–1199.

Macke, A., J. Mueller, and E. Raschke, 1996: Single scattering properties of atmospheric ice crystals. *J. Atmos. Sci.*, **53,** 2813–1825.

Mishchenko, M. I., and L. D. Travis, 1997: Satellite retrieval aerosol properties over the ocean using polarization as well as intensity of reflected sunlight. *J. Geophys. Res.*, **102,** 16 989–17 013.

Nicolas, F., L. R. Bissonnette, and P. H. Flamant, 1997: Lidar effective multiple-scattering coefficients in cirrus clouds. *Appl. Opt.*, **36,** 3458–3468.

Sassen, K., 1991: The polarization lidar technique for cloud research: A review and current assessment. *Bull. Amer. Meteor. Soc.*, **72,** 1848–1866.

——, and K. N. Liou, 1979a: Scattering of polarized laser light by water droplet, mixed-phase and ice crystal clouds. Part I: Angular scattering patterns. *J. Atmos. Sci.*, **36,** 838–851.

——, and ——, 1979b: Scattering of polarized laser light by water droplet, mixed-phase and ice crystal clouds. Part II: Angular depolarizing and multiple-scattering behavior. *J. Atmos. Sci.*, **36,** 852–861.

——, and Coauthors, 1995: The 5–6 December 1991 FIRE IFO II jet stream cirrus case study: Possible influences of volcanic aerosols. *J. Atmos. Sci.*, **52,** 97–123.

——, J. Campbell, and J. F. Barnett, 1998: Midlatitude cirrus clouds: A climatology from 10-year polarization lidar observation program at FARS. *Proc. 19th Int. Laser Radar Conf.*, Annapolis, MD, NASA, 45–46.

Sauvage, L., H. Chepfer, V. Trouillet, P. H. Flamant, G. Brogniez, J. Pelon, and F. Albers, 1999: Remote sensing of cirrus radiative parameters during EUCREX'94. Case study of 17 April 1994. Part I: Observations. *Mon. Wea. Rev.*, **127,** 486–503.

Spinhirne, J. D., A. R. Rall, and V. S. Scott, 1995: Compact eye-safe lidar systems. *Rev. Laser Eng.*, **23,** 112–118.

van de Hulst, H. C., 1981: *Light Scattering by Small Particles.* Dover Publications, 470 pp.

Vesperini, M., F. M. Bréon, and D. Tanré, 1999: Atmospheric water vapor content from spaceborne POLDER measurements. *IEEE Trans. Geosci. Remote Sens.*, **37**, 1613–1619.

Young, S., 1995: Analysis of lidar backscatter profiles in optically thin clouds. *Appl. Opt.*, **34,** 7019–7031.